

# Journal of Biomedical Optics

[SPIEDigitalLibrary.org/jbo](http://SPIEDigitalLibrary.org/jbo)

## **Performance assessment of an opto-fluidic phantom mimicking porcine liver parenchyma**

Tony J. Akl  
Travis J. King  
Ruiqi Long  
Michael J. McShane  
M. Nance Ericson  
Mark A. Wilson  
Gerard L. Côté

# Performance assessment of an opto-fluidic phantom mimicking porcine liver parenchyma

Tony J. Akl,<sup>a</sup> Travis J. King,<sup>a</sup> Ruiqi Long,<sup>a</sup> Michael J. McShane,<sup>a</sup> M. Nance Ericson,<sup>b</sup> Mark A. Wilson,<sup>c,d</sup> and Gerard L. Coté<sup>a</sup>

<sup>a</sup>Texas A&M University, Department of Biomedical Engineering, 5045 Emerging Technologies Building, 3120 TAMU, College Station, Texas 77843-3120

<sup>b</sup>Oak Ridge National Laboratory, P.O. Box 2008, MS 6006, Oak Ridge, Tennessee 37831-6006

<sup>c</sup>University of Pittsburgh, Department of Surgery, 200 Lothrop Street, Pittsburgh, Pennsylvania 15213

<sup>d</sup>University Dr. C-1w142, Veterans Affairs Healthcare System, Pittsburgh, Pennsylvania 15240

**Abstract.** An implantable, optical oxygenation and perfusion sensor to monitor liver transplants during the two-week period following the transplant procedure is currently being developed. In order to minimize the number of animal experiments required for this research, a phantom that mimics the optical, anatomical, and physiologic flow properties of liver parenchyma is being developed as well. In this work, the suitability of this phantom for liver parenchyma perfusion research was evaluated by direct comparison of phantom perfusion data with data collected from *in vivo* porcine studies, both using the same prototype perfusion sensor. *In vitro* perfusion and occlusion experiments were performed on a single-layer and on a three-layer phantom perfused with a dye solution possessing the absorption properties of oxygenated hemoglobin. While both phantoms exhibited response patterns similar to the liver parenchyma, the signal measured from the multilayer phantom was three times higher than the single layer phantom and approximately 21 percent more sensitive to *in vitro* changes in perfusion. Although the multilayer phantom replicated the *in vivo* flow patterns more closely, the data suggests that both phantoms can be used *in vitro* to facilitate sensor design. © 2012 Society of Photo-Optical Instrumentation Engineers (SPIE). [DOI: 10.1117/1.JBO.17.7.077008]

Keywords: implantable sensor; liver transplant; microfluidics; polydimethylsiloxane; telemetry; tissue phantom.

Paper 11770 received Dec. 20, 2011; revised manuscript received Jun. 6, 2012; accepted for publication Jun. 14, 2012; published online Jul. 11, 2012.

## 1 Introduction

According to the Organ Procurement and Transplantation Network (OPTN), as of July 2011, the number of patients on the national waiting list for a liver transplant is 16,169, while the number of procedures performed in 2011 is 2,037 (based on OPTN data as of July 22, 2011). These numbers suggest that the availability of donor organs is failing to meet the demands. Another issue that affects the demand for organs is the success rate of transplant procedures. One-year graft (Table 9.8a of Ref. 1) survival rates of patients receiving a liver from a deceased donor and living donor between 2006 and 2007 were 84.3% and 86.6%, respectively.<sup>1</sup> Clearly, there is a need to minimize graft loss to increase the success rate of liver transplants, which would also decrease the demand for organs. Graft loss mainly results from ischemia and is a common cause of transplant failures. Our group is developing an implantable perfusion and oxygenation sensor to monitor the health of a transplanted organ during the two-week post-transplant period.<sup>2</sup> We believe an implantable sensor can increase graft and patient survival rates by detecting trends in perfusion and oxygenation that suggest a failing organ and by sending an alert to the medical staff before the damage becomes irreversible.

Current perfusion monitoring methods include laser Doppler flowmetry, Doppler ultrasound, thermal diffusion, diffuse correlation spectroscopy (DCS), diffuse reflectance spectroscopy

(DRS), and near-infrared spectroscopy of indocyanine green (ICG) uptake.<sup>3-15</sup> Doppler-based methods involve measuring the Doppler shift induced by moving objects, such as red blood cells in the blood stream, and correlating the resulting Doppler shift to the flow. However, these sensors are bulky, not developed for total implantation, and are highly susceptible to motion artifact.<sup>3</sup> Thermal Diffusion is a technique, originally introduced by Bowman et al.<sup>6</sup> that measures local tissue perfusion based on thermal convection. A typical thermal diffusion probe consists of a proximal and a distal thermistor. The proximal thermistor measures the baseline temperature of the surrounding tissue, and the distal thermistor is powered to induce a slight temperature increase in the local tissue. The power required to maintain this temperature increase is a function of perfusion. Although this technique is capable of measuring perfusion in localized tissue, it is difficult to apply directly to blood vessels, which would be useful in monitoring graft health and, although the probes are small, they are tethered to a benchtop device not suitable for implantation. DCS and DRS are often combined to simultaneously measure oxygenation and perfusion levels of the blood. DCS measures the decay rate of the electric field autocorrelation function of light multiply scattered from turbid media and correlates this decay rate to the flow rate of the turbid media. While DCS and DRS are capable of measuring perfusion and oxygenation, the devices have not been miniaturized for implantation.<sup>10-12</sup> ICG is a dye with a characteristic absorption peak near the hemoglobin isobestic point (805 nm). Its clearance from the blood stream by liver tissue is measured

Address all correspondence to: Gerard L. Coté, Texas A&M University, Department of Biomedical Engineering, 5045 Emerging Technologies Building, 3120 TAMU, College Station, Texas 77843-3120. E-mail: [gcote@tamu.edu](mailto:gcote@tamu.edu)

by near-infrared spectroscopy, and its concentration in the blood stream versus time can be used to predict perfusion in the liver.<sup>13–15</sup> However, this technique requires the contrast agent, which is not a viable solution for continual monitoring over two weeks. While the aforementioned methods are capable of monitoring blood perfusion in the liver, due to size, cost, need for a contrast agent, and/or lack of oxygenation information, they are not suitable for implantation or for continuous, real-time monitoring of perfusion and oxygenation over a two-week period.

One specific method that has been clinically accepted as a means for monitoring oxygen saturation is pulse oximetry. Throughout the past two decades, pulse oximetry has been increasingly used to monitor systemic oxygen saturation in the clinical setting.<sup>16,17</sup> Light within the 600- to 900-nm wavelength range is capable of penetrating fairly deep into tissue. Due to the optical properties of tissue within this wavelength range, the reflectivity of light can be used to measure the perfusion and oxygenation of blood within the volume of tissue being probed. Oximetry utilizes the technique of measuring the reflectivity or transmission of light in a tissue volume based on the differences in the absorbance spectrum of oxygenated hemoglobin (HbO<sub>2</sub>) and deoxygenated hemoglobin (Hb) on both sides of the hemoglobin isobestic point (805 nm). The measured reflectivity or transmission of light at the two wavelengths is correlated to the oxygen saturation of the blood volume being probed.<sup>16,18,19</sup>

Our approach is based on miniaturization of a reflectance pulse oximetry technique, with the addition of a third wavelength at the hemoglobin isobestic point (805 nm) to separate oxygenation from perfusion.<sup>2,20–22</sup> When oxygenation is held constant and the perfusion changes, the pulsatile absorption of light due to hemoglobin is a function of the volume of blood present with each pulse and not the oxygen saturation of the hemoglobin. In cases of simultaneous change in perfusion and oxygenation, the isobestic wavelength (805 nm) will only monitor changes due to perfusion and can be used as a feedback signal to an adaptive filter that can extract oxygenation changes as shown previously by our group.<sup>21</sup> Since our sensor operates in the reflectance mode, it can be placed on both large blood vessels and capillary beds in tissue, such as the portal vein and liver parenchyma, to measure oxygenation and perfusion, metrics used to assess the health of a transplanted organ. Our sensor features a three-wavelength source (735, 805, and 940 nm) with dark current subtraction to eliminate noise from background light sources. The diffusely reflected light is collected by a silicon photo-detector. Figure 1 displays a schematic of the probe head of the sensor system used for the *in vitro* and *in vivo* studies.

The liver has a complex microcirculation divided into lobules, ~1-mm hexagonal structures, made of radial sinusoids (~10  $\mu$ m channels). In a reflectance optical sensor, this structure governs the signal strength due to the difference in scattering properties between blood and tissue. A phantom that can mimic this structure along with the optical and flow properties is essential for accurate testing of similar optical sensors while minimizing animal studies. Such a phantom can also be used for assessing optical imaging modalities. A phantom developed by our group<sup>23</sup> has been shown to mimic the optical properties of the liver parenchyma in the 630- to 1000-nm wavelength range. In this paper, the use of this phantom as a substitute for liver parenchyma is evaluated by direct comparison of perfusion sensor data to results collected from *in vivo* porcine studies.

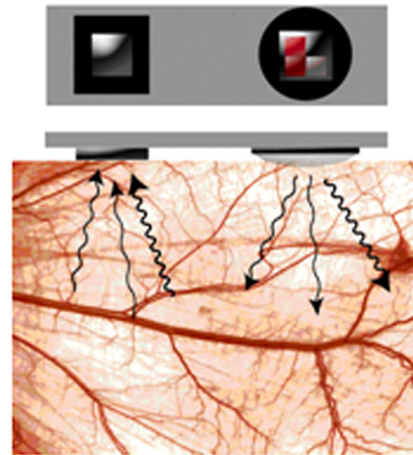


**Fig. 1** Schematic of the sensor system used for the *in vitro* and *in vivo* perfusion studies. The three arrows represent the three different wavelengths of light emitted by the source.<sup>20</sup>

## 2 Materials and Methods

### 2.1 Phantom Fabrication

The phantom fabrication process has been previously described in detail by our group.<sup>23</sup> Briefly, it consists of two main steps: mold fabrication and polydimethylsiloxane (PDMS) preparation. The micro-channels' molds are made of SU-8, and they mimic the structure of the liver microcirculation (Fig. 2). Each lobule, 1 mm in diameter, is made of 18 radial micro-channels, 15  $\mu$ m in width and 50  $\mu$ m in depth. Every mold corresponds to one layer of micro-channels and has a total of 20- $\times$ -20 lobules with two input channels and one output channel to mimic the dual blood supply to the liver (hepatic artery and portal vein). The recipe to make the phantoms was designed to mimic the optical properties of porcine liver tissue. Aluminum oxide powder with two different size distributions (0.5 to 1  $\mu$ m and 100 nm) was mixed with uncured PDMS at a concentration of 7.29 and 2 mg/mL, respectively. For every 1 mL of PDMS, 0.67  $\mu$ L of black India ink (Black India 4415, Higgins®) and 2  $\mu$ L of blue #1 food coloring (Wilton®) was added. The mixture was sonicated and stirred intermittently until it became homogeneous. The curing agent was added at a volumetric ratio of 10:1, and the mixture was stirred and degassed in a vacuum chamber to remove air bubbles. A precalculated volume of the recipe, which corresponds with the desired thickness of each layer, was dispensed on the SU-8 molds to form the micro-channels or in a petri-dish to form the bottom base layer. The mixtures were degassed again to remove bubbles entrapped in the microchannels, and placed in a preheated oven at 65°C to pre-cure for 50 min. The micropatterned PDMS and the base layer were corona treated and bonded to each other. We used 20-gauge syringe needles to access the input and output channels of each layer. In the case of the multilayer phantom, three micropatterned layers were used and aligned as shown in panel (b) of Fig. 2. The phantoms were then placed back in the oven for a final bake for 70 min.

### 2.2 In Vitro System Setup

To assess how well the single and multilayer phantoms mimic the flow properties of liver parenchyma, we assembled an *in vitro* system to control and measure changes in perfusion.

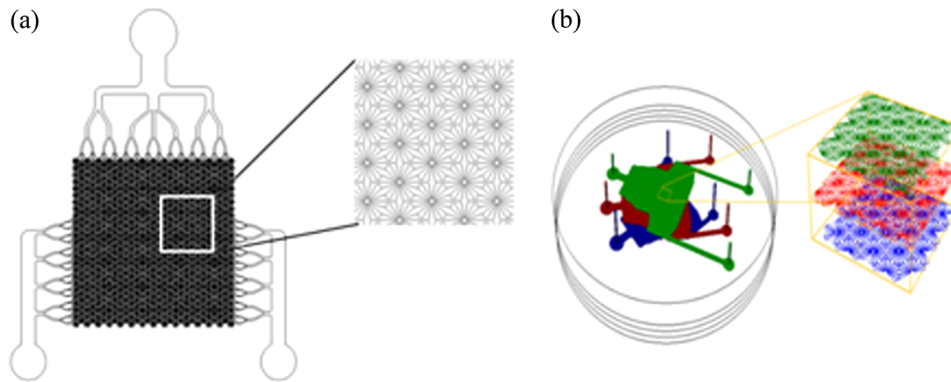


**Fig. 2** (a) 2-D pattern design of the microfluidic channels for a single layer; (b) assembly of three layers to form the multilayer phantom.

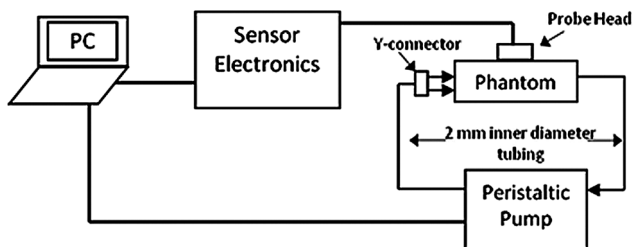


**Fig. 3** *In vitro* system diagram used to perform perfusion and occlusion experiments.

The *in vitro* setup consisted of a peristaltic pump, the parenchymal phantom, and a dye solution (Fig. 3).

Each layer of channels contains two input ports and one output port to allow fluid to be pulsed through the phantoms. The two input ports mimic the branches of the portal vein and hepatic artery that supply blood to the lobules from the portal triad, and the output port mimics the branch of the hepatic vein that drains the filtered blood from the lobules. To avoid the complications associated with maintaining whole blood oxygen saturation and other variables over time, we used a dye solution made of a mixture of diluted India ink and Epolight 2717 in phosphate buffered saline (PBS) that mimics the absorption of oxygenated blood at our wavelengths of interest (735, 805, and 940 nm).<sup>24</sup> More specifically, the India ink (Black India 44120, Higgins) was dissolved in 0.01 M phosphate buffered saline (PBS; pH 7.4) at a concentration of 0.88% *v/v*. The India ink solution was then filtered through a 0.45- $\mu\text{m}$  syringe filter (VWR, cat. # 28145-481) to remove larger particles that could clog the microfluidic channels, and the absorption spectrum of the filtered India ink solution was measured using a spectrophotometer (Hitachi U4100, Hitachi). After measuring the absorption spectrum of the filtered India ink solution, Epolight 2717<sup>TM</sup> (Epolin) was added at a concentration of 0.304 mg/mL so that the absorption spectrum of the solution matched the absorption spectrum of the oxygenated hemoglobin at our wavelengths of interest. The absorption of the dye solution at 735 nm was higher than the absorption of HbO<sub>2</sub> (Table 1). However, this was not problematic for this study because the same dye solution was used for all studies, and simulations involved varying perfusion and not oxygenation.

A peristaltic pump (Minipuls 3; Gilson), which produced a pulsatile flow pattern, pumped the dye solution through the phantoms. The pump was driven via a data acquisition unit

**Table 1** Extinction coefficients of the dye solution and oxygenated hemoglobin at the wavelengths of interest.<sup>25</sup>

$\lambda$	Oxy dye solution $\mu\text{a}$ ( $\text{cm}^{-1}$ )	HbO <sub>2</sub> $\mu\text{a}$ ( $\text{cm}^{-1}$ )
735 nm	4.23	2.408
805 nm	4.789	4.557
940 nm	6.46	6.555

(National Instruments, USB-6009) and a custom program developed using LabVIEW software (National Instruments). The driver signal for the peristaltic pump was a square wave, and the pump frequency was set to mimic the cardiac pulsatile flow pattern. Output flow from the pump was determined by the pump drive rates and tubing size. Before the phantoms were connected to the peristaltic pump, the dye solution was loaded into the phantoms using two syringe pumps. The first syringe pump (cat. # 70-2208, Harvard Apparatus) was connected to the input ports and set to pump at a volumetric flow rate of 0.3 and 0.9 mL/min for the single and multilayer phantom, respectively, and the second syringe pump (New Era Pump Systems, Inc., NE-4000) was connected to the output ports and set to withdraw at a rate of 0.35 and 0.95 mL/min for the single and multilayer phantom, respectively, creating a negative pressure gradient to help perfuse the phantoms without bursting the connections at the input and output ports.

For the perfusion measurements, the pump frequency was set at 100 beats per minute to approximate the cardiac pulsatile flow rate of the *in vivo* porcine data. The volumetric flow rate of the peristaltic pump was varied within the range of physiological rates for a section of liver parenchyma containing the same number of lobules as the single and multilayer phantoms. The average volumetric flow rate of the liver is 1450 mL/min (~1 mL/min/gm of tissue), and the human liver contains on average roughly 1 million lobules.<sup>26,27</sup> By dividing the average mass of the liver (1.5 kg)<sup>28</sup> by the number of lobules, the mass per lobule was calculated (1.5 mg/lobule). Using the average lobule mass and the flow per gram of tissue, the flow through one lobule was calculated to be 1.5  $\mu\text{L}/\text{min}$  per lobule. Each layer in the designed phantoms is made of 400 lobules leading to a flow of 0.6 mL/min per layer. These values were used to pump the dye solutions through the phantoms.

The probe used to collect data was circular in design (1 inch in diameter) and contains a four-wavelength LED (Epitex, L660/735/805/940-40B42-C-I) wired to deliver three wavelengths of light (735, 805, and 940 nm) and a silicone photodetector (S2833-01, Hamamatsu). The source to detector separation (edge to edge) of the probe used in this study was 2 mm.<sup>24,29</sup> The probe was fixed to the surface of the phantoms with a mechanical arm and coupling gel (G608N, Thorlabs) was applied to the surface of the LED and photodetector to enhance the light coupling to the surface of the PDMS-based phantom.

### 2.3 In Vivo Occlusion Studies

A female swine was premedicated with Telazol (5 to 10 mg/kg) and Buprenorphine (0.01 to 0.05 mg/kg) intramuscularly (IM) for approximately 15 min prior to induction of anesthesia. Anesthesia was induced with Isoflurane (~3% to 4%) in oxygen at a rate of 3 L/min via a face-mask. The subject was then intubated with an appropriately sized endotracheal tube according to the approved animal use protocol. Anesthesia was maintained with Isoflurane (0.5% to 4%) in oxygen (15 mL/lb, maximum 5L). A pulse oximetry probe was placed on the swine to monitor SpO<sub>2</sub>. The animal was then connected to a ventilator and mechanical respiration was provided at a rate of eight to 12 breaths per minute and tidal volume of 5 to 10 mL/lb.

A laparotomy was performed for exposure of the liver, and the probes were placed on the right and left lobe of the liver parenchyma, on the portal vein, and on the hepatic artery via sutures. A thermal diffusion probe (Bowman Perfusion Monitor; Hemedex, Inc.) was placed the liver parenchyma to measure blood perfusion. Vascular occluders were placed around the portal vein and hepatic artery for use with the vascular occlusion studies. Before occlusion of each vessel, at least one baseline signal was collected for 60 s. The inhaled oxygen concentration was kept constant during these studies and the SpO<sub>2</sub> readings from the pulse oximeter were monitored to make sure the blood oxygen saturation was constant throughout the occlusion study. The data segments were analyzed using FFT analysis.

## 3 Results

### 3.1 In Vitro Results

Figure 4 displays 10-s segments of the time-domain AC signal measured using the sensor described in Sec. 1 on the single layer parenchymal phantom [4(a)], multilayer parenchymal phantom [4(b)], and liver parenchyma [4(c)]. Also shown in Fig. 4 are the corresponding FFT plots of 60-s data segments (each consisting of 1800 data points) gathered with the sensor system on the single layer parenchymal phantom [4(d)], multilayer parenchymal phantom [4(e)], and liver parenchyma [4(f)]. The FFT spectrum

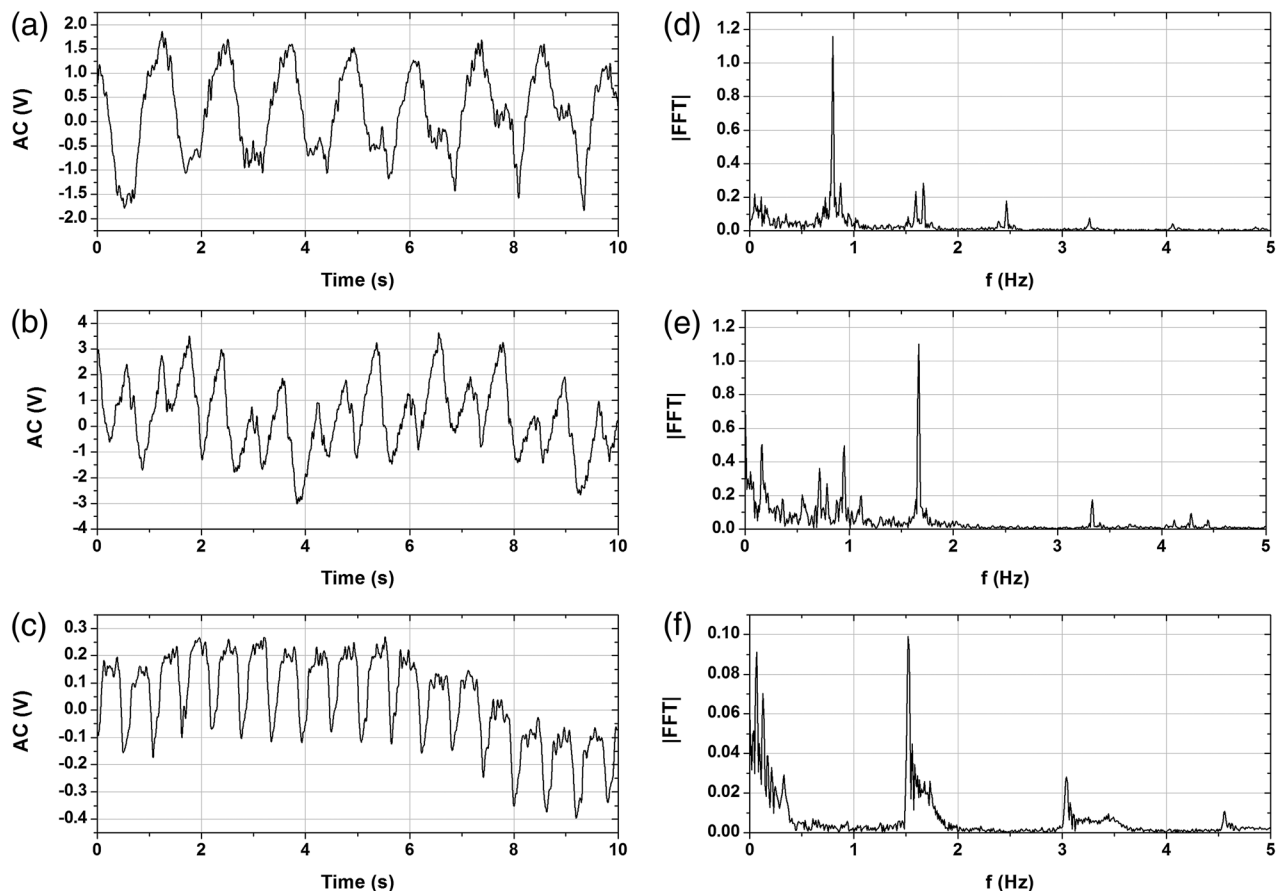


**Fig. 4** Ten-second segment of the time-domain AC signal measured from the single layer parenchymal phantom (a), multilayer parenchymal phantom (b), and porcine liver parenchyma (c). The corresponding FFT spectrum for a 60-s sampling of data is shown in the right column for each case, and shows the 1.667-Hz frequency due to the pulse frequency. Note there is a subharmonic at 0.8 Hz in the phantom frequency data, which is due to back flow caused by pressure buildup. Also seen are the harmonics of the 1.667-Hz signal seen at 3.334 Hz.

of the *in vitro* data contains a peak at 1.667 Hz corresponding to the pulse frequency (100 bpm) of the peristaltic pump as well as harmonics seen at 3.334 Hz. The data shows the ability of the phantom to mimic the pulsatile flow seen *in vivo* at perfusion levels similar to the normal physiologic rates in healthy individuals. The spectra from the phantom shown in Fig. 4 indicate the presence of an additional lower frequency component at 0.833 Hz. The origin of this signal was back flow due to increased pressure in the circulation as described in detail in the “Discussion” section. This noise signal is dependent on the mechanical properties of the different components in the perfusion system (phantom and tubing compliances). These parameters can be varied to minimize this noise. By adjusting the mechanical properties this noise phenomenon can be used to mimic the back pressure artifact seen *in vivo* at these lower frequencies due to respiration and this information can be used to develop algorithms to separate cardiac signal from respiratory artifacts in our sensing system.

As the amount of blood present per pulse decreases or increases, the pulsatile absorption due to the presence of the blood also decreases or increases, respectively, for each of the three wavelengths (735, 805, and 940 nm). This change in the absorption corresponds to a change in the amplitude of the AC signal and an accompanying change in the FFT peak value at the pulse frequency. Figure 5 displays a plot of the FFT peak value as a function of perfusion for the single layer parenchymal phantom. All values were normalized to the FFT peak at the highest flow. At each wavelength, the FFT peak

value increases linearly with an increase in the volumetric flow of the dye solutions. The linear fit to the data collected at 735, 805, and 940 nm has a slope of 1.07, 1.08, and 1.09, respectively, indicating that the absorption due to each wavelength increases at approximately the same rate with an increase in perfusion. This trend is expected since the volume per pulse, not the oxygen saturation, of the dye solution is changing in this experiment.

Figure 6 displays the FFT peak value as a function of perfusion for the multilayer parenchymal phantom. As with the single layer phantom, the FFT peak values increase linearly with an increase in perfusion at each wavelength. The slope of the fit lines for the 735, 805, and 940 nm wavelengths is 1.40, 1.36, and 1.34, respectively, indicating that the absorption at each wavelength is increasing at approximately the same rate with an increase in perfusion. This is consistent with the data from the single layer parenchymal phantom. However, the signal increases observed with the multilayer phantom were greater than the single layer phantom indicating a greater sensitivity to changes in perfusion for the data collected from the multilayer phantom. The multilayer phantom was expected to have a higher sensitivity to volumetric flow changes due to the presence of a higher overall volume of blood resulting from more lobules present than the single layer phantom (1200 versus 400 lobules).

To assess how well the phantom mimics the flow characteristics of liver parenchyma, *in vitro* occlusion studies were performed to simulate blockage of flow to the liver by reducing the flow on the input ports of the phantoms. For these studies

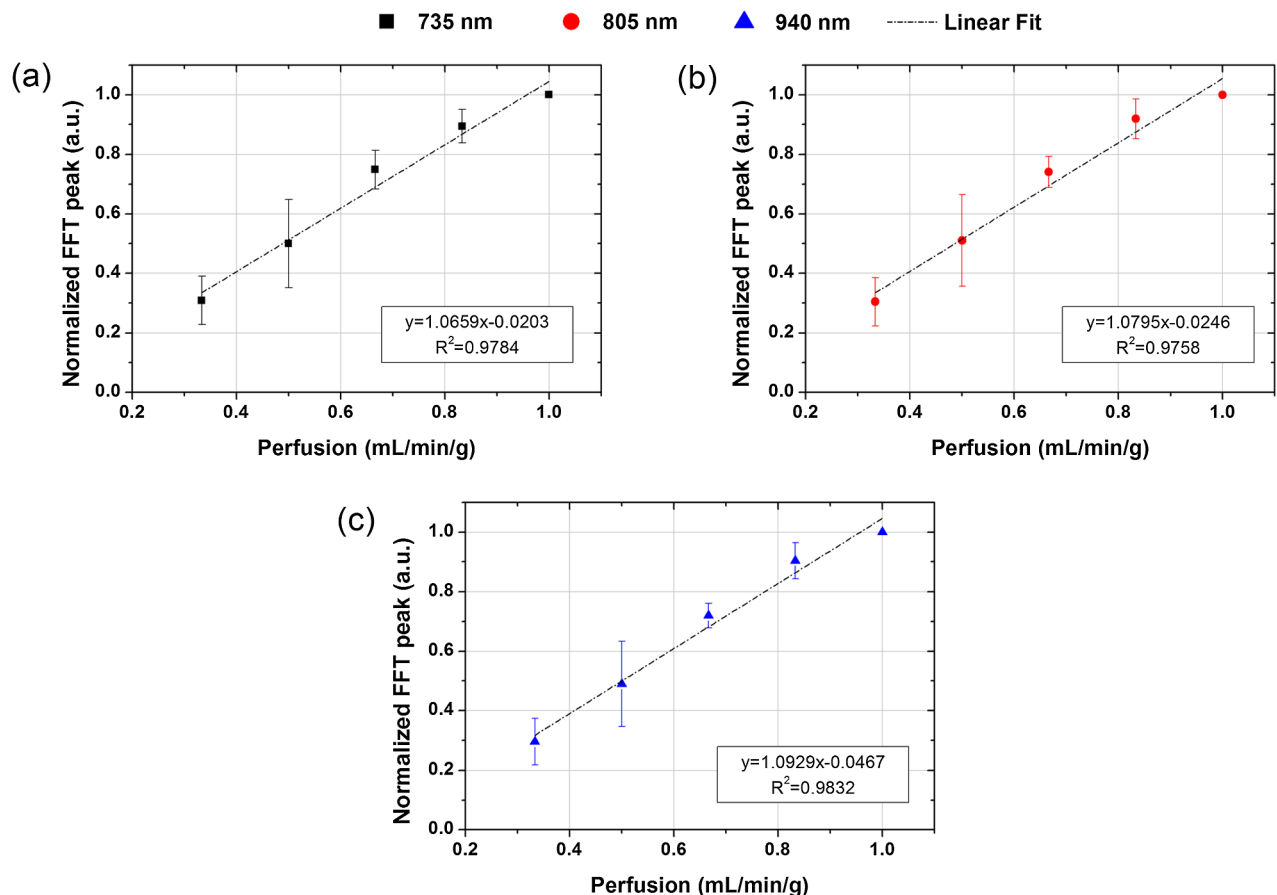


**Fig. 5** Normalized FFT peak value at 1.667 Hz (100 bpm) for 735 nm (a); 805 nm (b); and 940 nm (c) versus volumetric flow for the single layer parenchymal phantom. The error bars indicate  $\pm$  one standard deviation from three separate experiments.

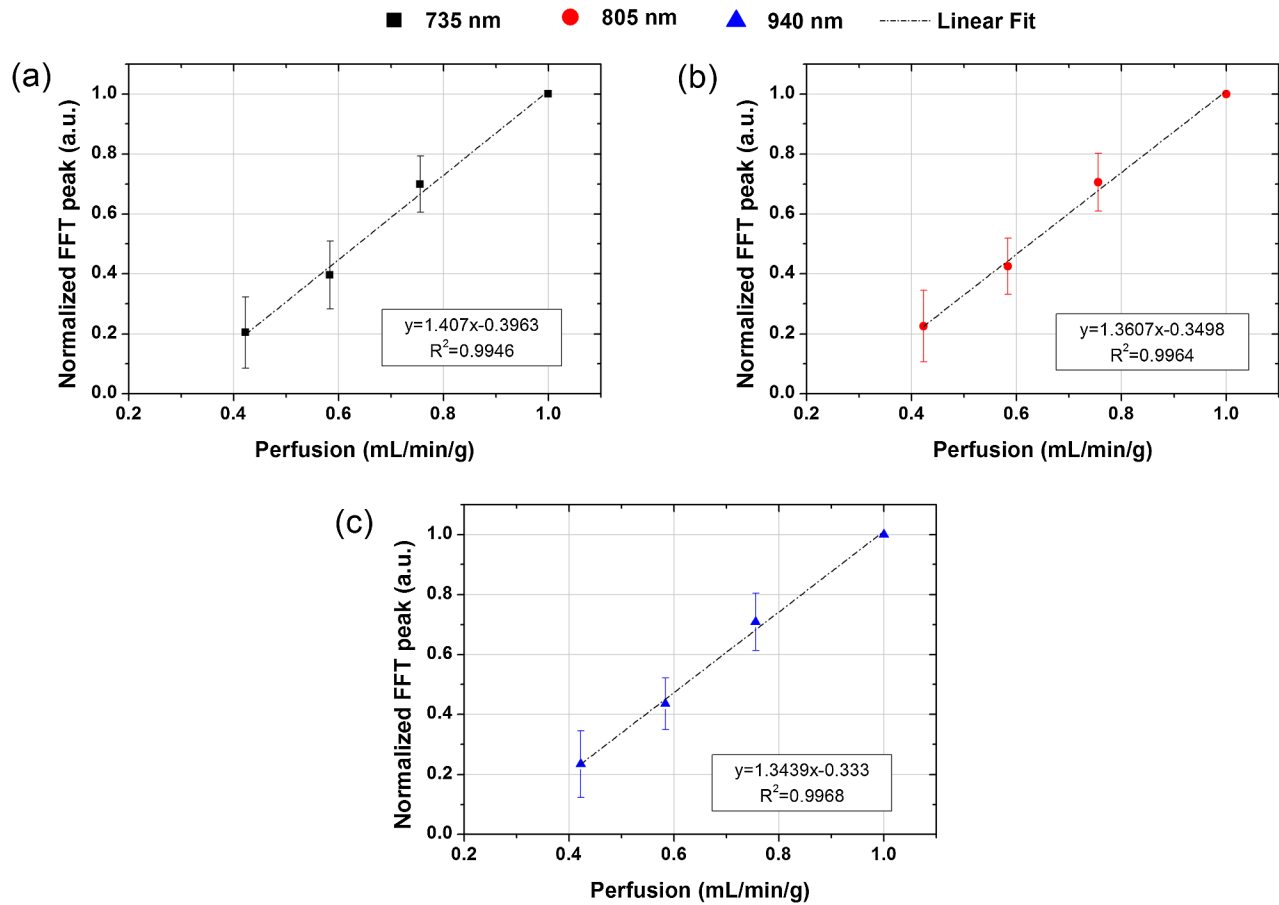


Fig. 6 Normalized FFT peak value at 1.667 Hz (100 bpm) for 735 nm (a); 805 nm (b); and 940 nm (c) versus volumetric flow for the multilayer parenchymal phantom.

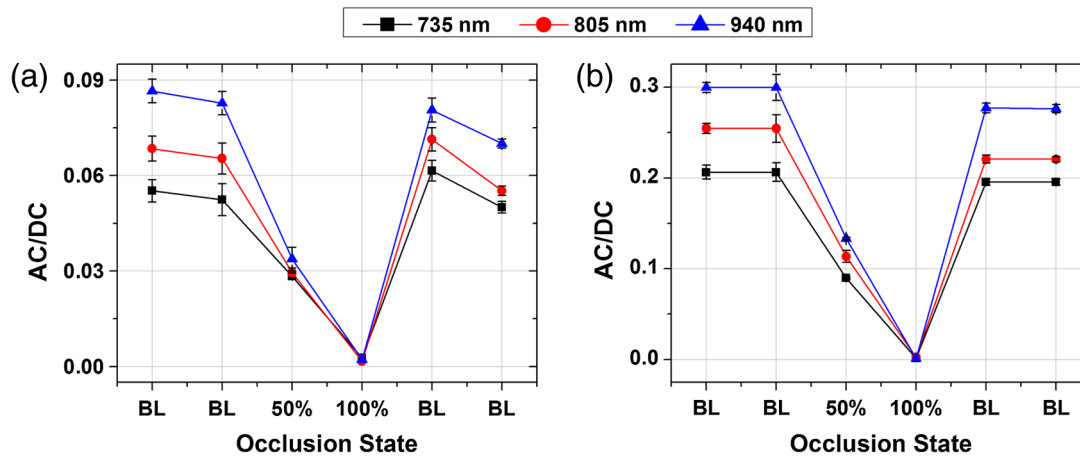
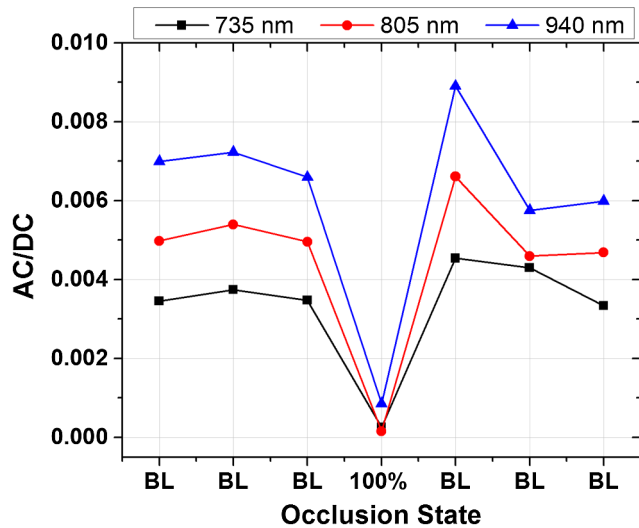


Fig. 7 *In vitro* occlusion studies performed on (a) the single layer parenchymal phantom and (b) multilayer parenchymal phantom showing a decrease in signal during occlusion of the inputs to the phantoms and an increase in signal as perfusion is restored.

volumetric flows mimicking 50% and 100% occlusion of flow were used to compare occlusion in the phantoms to the *in vivo* liver experiments and to evaluate the response of the phantoms and the performance of the sensor system during conditions of hypo-perfusion. The peristaltic pump was set to pump at the physiologic flow rate for a section of 400 lobules for the single layer phantom and 1200 lobules for the multilayer phantom to record the baseline signal. This is represented in Fig. 7(a) (single layer phantom) and 7(b) (multilayer phantom) as the first two

data points. Each data point is the FFT peak value computed from 60 s of raw data, divided by the measured DC voltage. To simulate a 50% occlusion, the peristaltic pump was adjusted so that the volumetric flow was 50% of the flow used for the baseline value. To simulate total occlusion, the peristaltic pump was turned off so that no flow existed in the phantoms. After simulation of total occlusion, the volumetric flow of the pump was restored to the baseline value and two more sets of data were collected. During 50% occlusion, the signal at each



**Fig. 8** *In vivo* occlusion studies showing a decrease in signal during total occlusion (100%) and an increase in signal as perfusion is restored.

wavelength decreases, indicating a decrease in the volume of dye solution present. During 100% occlusion the signal at each wavelength is zero, indicating no dye solution flow. The final baseline points indicate the ability of the phantoms to recover during restored flow. It must be noted that the experiments were performed using the dye solution that mimicked 100% oxygen saturation, which explains the greater signal amplitude observed for the 940 nm wavelength as compared to the other wavelengths.

### 3.2 *In Vivo* Results

For the *in vivo* occlusion study, a total occlusion was created by the use of mechanical occluders on both the portal vein and hepatic artery. Figure 8 displays the results of the *in vivo* occlusion studies. During full occlusion the signal at each wavelength decreased to nearly zero, indicating a significant decrease in blood flow. Also, the signal recovered to baseline after full flow was restored.

## 4 Discussion

During changes in perfusion, the absorption due to blood is dependent on the volume of blood present during each pulse rather than the oxygen saturation of the blood. Reduction in blood perfusion produces a lower modulation of light absorbed by the blood, due to the reduced modulation of the blood volume, resulting in a lower AC signal measured at the perfusion sensor. A change in oxygen saturation results in an increase and simultaneous decrease in absorption at wavelengths on opposite sides of the isobestic point (805 nm) while the absorption at this isobestic point remains constant. In this manner, a change in perfusion can be distinguished from a change in oxygen saturation. This change in perfusion was observed during *in vitro* studies performed on a single layer and multilayer phantom mimicking the structure of liver parenchyma and *in vivo* studies performed on a female swine.

With a change in perfusion, the slopes of the linear fit for all three wavelengths for the single layer phantom were nearly identical, while the same was true for each of the wavelengths for the multilayer phantom. However, the slope varied between the two types of phantoms. The average of the slope of the linear fit for

the data from the multilayer phantom was 21% higher than that of the single layer phantom indicating a greater sensitivity to changes in perfusion in the multilayer phantom. A higher signal was expected due to the presence of a larger volume of blood in the multilayer phantom. While the perfusion was identical per gram of “tissue,” the multilayer phantom contains more hexagonal structures mimicking liver lobules than the single layer phantom (1200 versus 400). Therefore, with each pulse, a higher overall volume of the dye solution was present in the multilayer phantom, affecting the AC signal. Also, the increased ambient volume of blood causes a change in the DC signal.

As with the *in vivo* experiments, we were able to measure an AC signal in both phantoms at the same frequency as the peristaltic pump (Fig. 4). However, the ratio of AC to DC is slightly higher in the multilayer phantom. This observation was expected because the multilayer phantom contains more hexagonal structures and can hold a higher volume of dye solution. The increased volume of dye solution causes a greater volume difference between the pulse state and the rest state in the multilayer phantom than in the single layer phantom. Also, the increased amount of dye solution present during the resting state causes more of the light to be absorbed causing a decrease in the DC voltage measured by the sensor. Therefore, an increase in the AC voltage along with a decrease in the DC voltage causes the ratio to increase. Although the AC/DC in the multilayer is slightly higher than the AC/DC in the single layer phantom, the AC waveform of the multilayer phantom is less uniform due to the presence of three layers of hexagonal structures fed through three separate channels.

With each phantom, the signal decreased with a simulation of 50% and 100% occlusion of the inputs to the phantoms. The same phenomenon was observed during the *in vivo* occlusion studies (Fig. 8), specifically, 100% occlusion of flow to the liver. The signal at each wavelength decreases to nearly zero before recovering to approximately the same baseline value after flow was fully restored. At 50% occlusion, the ratio for the single layer phantom was slightly lower than half of the baseline value, while the ratio was exactly half of the baseline value for the multilayer phantom. A greater signal magnitude was also observed for the multilayer phantom in comparison to the signal of the single layer phantom. The signal observed during the occlusion studies at each wavelength is nearly three times higher in the multilayer phantom than in the single layer phantom, which is feasible due to the presence of three times the amount of hexagonal structures in the multilayer phantom than in the single layer phantom.

Our results show that both the single and multilayer phantoms can be used to mimic, to some extent, perfused liver tissue. The multilayer phantom gave a stronger signal, and more layers would likely increase the signal even higher until the layers are thicker than the penetration depth of our light sources. Although adding more layers is possible, it is challenging to fabricate, align, and bond the silicone material with more layers and is further complicated by the number of input and output ports that would be required. The three-layer phantom has nine input/output ports connected to external tubes. This number increases by three for every added layer.

The measured signal from the phantoms had a low frequency component (around 0.833 Hz) that corresponds to back flow due to pressure build up in the circulation system. To verify this hypothesis, since our measurements are not sensitive to flow direction, air bubbles were introduced in the circulation and

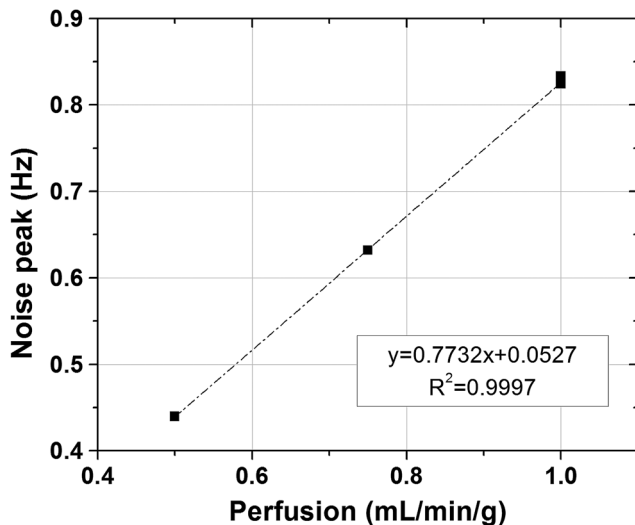


**Fig. 9** Back-pressure peak frequency as a function of perfusion levels for the single layer phantom. Note that the plot has 16 data points at three different flow levels but most of these points are overlapping.

the flow pattern monitored visually. In this experiment, back flow was depicted at the corresponding frequency. To better understand this phenomenon, the flow levels were varied and the peak shifted in a linear fashion ( $R^2 = 0.9997$ ) as shown in Fig. 9. This was expected for higher flow levels since the pressure builds up faster and the frequency of the back flow was higher. Further, the amplitude of the peak did not correlate to the changes in flow level. This peak could be varied by adjusting the mechanical properties of the fluidic system either by changing the curing method of the PDMS as described by Hong et al.<sup>30</sup> or modifying the tubing (material or size) used in the system. Preliminary studies were conducted to verify this hypothesis, and the low-frequency peak was able to be shifted from 0.833 to 0.55 Hz at a constant perfusion level of 1 ml/min/g by using a more compliant phantom. This peak can be adjusted to mimic different noise artifacts seen *in vivo*.

## 5 Conclusions

Development of a phantom that not only has anatomical and optical properties similar to liver parenchyma but also mimics the functional perfusion for our sensor has been demonstrated. This will aid in facilitating sensor design while decreasing the number of animal studies needed. In this work, we compared perfusion data gathered from *in vitro* occlusion-mimicking experiments performed on a single and multilayered phantom that optically and anatomically mimics liver parenchyma to *in vivo* occlusion experiments performed on a female swine. We demonstrated the ability to measure a pulsatile signal with the parenchymal phantoms and to measure a peak in the FFT spectrum at 1.667 Hz corresponding to the pulse frequency of the peristaltic pump (100 bpm). The FFT peak value at each wavelength decreased as the perfusion of dye solutions decreased, a trend observed in both phantoms. We found that both phantoms displayed the same occlusion patterns as the *in vivo* case, but the signal acquired from studies on the multi-layer phantom was nearly three times higher and showed greater sensitivity than the signal acquired from studies on the single layer phantom. While these observations demonstrate the suitability of both parenchymal phantoms for use in the design of

the perfusion sensor, it is more appropriate to use the three-layer phantom because it more closely mimics the anatomical properties of liver parenchyma.

## Acknowledgments

This research was funded by a bioengineering research partnership (BRP) grant from NIH, (#5R01-GM077150). The data and analyses reported in the 2009 Annual Report of the U.S. Organ Procurement and Transplantation Network and the Scientific Registry of Transplant Recipients have been supplied by UNOS and Arbor Research under contract with HHS/HRSA. The authors alone are responsible for reporting and interpreting these data; the views expressed herein are those of the authors and not necessarily those of the U.S. Government.

## References

1. "2009 Annual Report of the U. S. Organ Procurement and Transplantation Network and the Scientific Registry of Transplant Recipients: Transplant Data 1999–2008," Department of Health and Human Services, Health Resources and Services Administration, Healthcare Systems Bureau, Division of Transplantation, Rockville, MD; United Network for Organ Sharing, Richmond, VA; University Renal Research and Education Association, Ann Arbor, MI (2009).
2. W. Ericson et al., "Implantable sensor for blood flow monitoring after transplant surgery," *Minim. Invasive Ther Allied Technol.* **13**(2), 87–94 (2004).
3. A. Humeau et al., "Laser Doppler perfusion monitoring and imaging: novel approaches," *Med. Biol. Eng. Comput.* **45**(5), 421–435 (2007).
4. H. P. Notzli et al., "Perfusion of the femoral head during surgical dislocation of the hip: monitoring by laser Doppler flowmetry," *J. Bone Joint Surg. Br.* **84-B**(2), 300–304 (2002).
5. C. Tziafalia et al., "Echo-Doppler measurements of portal vein and hepatic artery in asymptomatic patients with hepatitis B virus and healthy adults," *J. Gastrointest Liver Dis.* **15**(4), 343–346 (2006).
6. H. F. Bowman and T. A. Balasubramaniam, "A new technique utilizing thermistor probes for the measurement of thermal properties of biomaterials," *Cryobiology* **13**(5), 572–580 (1976).
7. M. B. Khot et al., "Thermal diffusion probe analysis of perfusion changes in vascular occlusions of rabbit pedicle flaps," *Plast. Reconstr. Surg.* **115**(4), 1103–1109 (2005).
8. G. T. Martin and H. F. Bowman, "Validation of real-time continuous perfusion measurement," *Med. Biol. Eng. Comput.* **38**(3), 319–325 (2000).
9. P. Vajkoczy et al., "Continuous monitoring of regional cerebral blood flow: experimental and clinical validation of a novel thermal diffusion microprobe," *J. Neurosurg.* **93**(2), 265–274 (2000).
10. D. A. Boas and A. G. Yodh, "Spatially varying dynamical properties of turbid media probed with diffusing temporal light correlation," *J. Opt. Soc. Am. A* **14**(1), 192–215 (1997).
11. Y. Shang et al., "Portable optical tissue flow oximeter based on diffuse correlation spectroscopy," *Opt. Lett.* **34**(22), 3556–3558 (2009).
12. C. Zhou et al., "Diffuse optical monitoring of hemodynamic changes in piglet brain with closed head injury," *J. Biomed. Opt.* **14**(3), 034015 (2009).
13. L. R. Jiao et al., "Effect of liver blood flow and function on hepatic indocyanine green clearance measured directly in a cirrhotic animal model," *Brit. J. Surg.* **87**(5), 568–574 (2000).
14. R. E. Stauber et al., "Evaluation of indocyanine green clearance and model for end-stage liver disease for estimation of short-term prognosis in decompensated cirrhosis," *Liver Int.* **29**(10), 1516–1520 (2009).
15. H. A. Wynne et al., "The effect of age upon liver volume and apparent liver blood flow in healthy man," *Hepatology* **9**(2), 297–301 (1989).
16. T. Aoyagi, "Pulse oximetry: its invention, theory, and future," *J. Anesthesia* **17**(4), 259–266 (2003).
17. J. G. Webster, *Design of Pulse Oximeters*, Institute of Physics Pub., Bristol, Philadelphia (1997).

18. P. D. Mannheim, "The light-tissue interaction of pulse oximetry," *Anesth. Analg.* **105**(On Line Suppl.), S10–17 (2007).
19. A. Jubran, "Pulse oximetry," *Crit. Care* **3**(2), R11–R17 (1999).
20. M. N. Ericson et al., "Development of an implantable oximetry-based organ perfusion sensor," in *Engineering in Medicine and Biology Society, 2004. IEMBS '04. 26th Annual International Conference of the IEEE*, Vol. **1**, pp. 2235–2238 (2004).
21. H. Subramanian et al., "Real-time separation of perfusion and oxygenation signals for an implantable sensor using adaptive filtering," *IEEE Trans. Biomed. Eng.* **52**(12), 2016–2023 (2005).
22. H. Subramanian et al., "An autocorrelation-based time domain analysis technique for monitoring perfusion and oxygenation in transplanted organs," *IEEE Trans. Biomed. Eng.* **52**(7), 1355–1358 (2005).
23. R. Long et al., "Optofluidic phantom mimicking optical properties of porcine livers," *Biomed. Opt. Express* **2**(7), 1877–1892 (2011).
24. T. J. Akl et al., "Optimizing probe design for an implantable perfusion and oxygenation sensor," *Biomed. Opt. Express* **2**(8), 2096–2109 (2011).
25. S. Prahl, *Optical Absorption of Hemoglobin* (1999).
26. R. V. Krstić, *Human Microscopic Anatomy: An Atlas for Students of Medicine and Biology*, Springer-Verlag, Berlin, New York (1991).
27. A. C. Guyton and J. E. Hall, and ScienceDirect, *Textbook of Medical Physiology*, Elsevier Saunders, Philadelphia (2006).
28. V. Kumar et al., *Robbins and Cotran Pathologic Basis of Disease*, Elsevier Saunders, Philadelphia (2005).
29. T. J. Akl et al., "Optimizing source detector separation for an implantable perfusion and oxygenation sensor," *Proc. SPIE* **7906**, 790605 (2011).
30. H. C. Hong et al., "Study of novel electrical routing and integrated packaging on bio-compatible flexible substrates," *Microsyst. Technol.* **16**(3), 423–430 (2010).